

**Tidal wave in ^{102}Pd :
Rotating condensate of up to seven d-bosons**

S. FRAUENDORF*, M. A. CAPRIO, and J. SUN

Department of Physics, University Notre Dame, IN 46557, USA

**E-mail: sfraue@nd.edu*

The yrast states of even even vibrational and transitional nuclei are interpreted as a rotating condensate of interacting d-bosons and the corresponding semi-classical tidal wave concept. A simple experimental manifestation of the anharmonicity caused by the boson interaction is found. The interpretation is substantiated by calculations based on the Collective Model and the Cranking Model.

Keywords: d-bosons, Collective Model, Cranking Model, transitional nuclei

1. Were to find the states with highest number of phonons?

The collective quadrupole excitations of nuclei are classified as "rotational" and "vibrational" with a rigid rotor and a harmonic vibrator being the limiting ideal cases. Rotational bands that extend over ten and more states are ubiquitous. Vibrational excitations of spherical nuclei are much less distinct. While the two-phonon triplet is often observed, identification of all members of the three-phonon multiplet is already problematic. Fig. 1 schematically shows the location of the vibrational states and of the quasiparticle excitations for a spherical nucleus. With increasing phonon number n , the collective states are embedded into a progressively dense background of quasiparticle excitations. The coupling to the quasiparticle background fragments the collective states, which cease to exist as individual quantum states. The density of quasiparticle excitations is lowest near the yrast line, which is the sequence of states with minimal energy for a given angular momentum I . With increasing phonon number n , the yrast members of the vibrational multiplets keep their identity as collective quantum states longest. Moreover, they couple to high- j two-quasiparticle excitations, which have a simple structure. Hence, the vibrational states with highest phonon

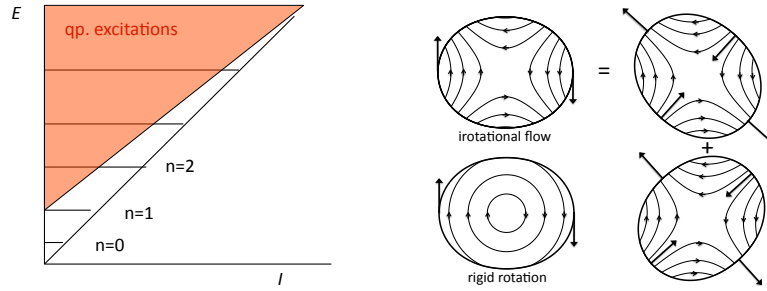


Fig. 1. Schematic excitation spectrum of a vibrational nucleus displayed for different angular momenta I . The states of minimal energy E for given I are indicated as the yrast line to the right.

Fig. 2. Flow pattern of a wave running about the surface of a drop of ideal liquid (upper left), standing waves (pulsating vibrations) of such a droplet (right), and a rigidly rotating body (lower left). The running (tidal) wave can be thought as a superposition of two standing waves pulsating with a phase shift of $\pi/2$. From Ref.².

number are expected at the yrast line. In this talk, we discuss $^{102}_{46}\text{Pd}_{56}$. The recent lifetime measurements by A. D. Ayangeakaa and U. Garg in collaboration with the ANL group,¹ have provided clear evidence for the identification of the seven-boson yrast state.

2. The tidal wave concept

If quadrupole vibrations are contrasted with rotation, one usually refers to the pulsating standing wave shown on the right hand side of Fig. 2. This mode represents the zero-angular momentum members of the vibrational multiplets, which are most rapidly drowned in the sea of quasiparticle excitations. The vibrational yrast states correspond to a wave that travels over the nuclear surface. The surface rotates with the constant angular velocity ω as in the case of the rotation of a rigid body. However, the flow pattern is irrotational. As characteristic for a surface wave, liquid moves from the wave front under the crest to the back side. The name "tidal wave" has been suggested for the yrast mode² because of its similarity with tidal waves on the ocean. The energy and the angular momentum increase with the amplitude of the wave, whereas the frequency stays constant. In the case of rigid rotation the energy and the angular momentum increase with the angular frequency while the shape remains unchanged.

The yrast line of vibrational nuclei consists of a sequence of stacked

d-bosons, which align their angular momenta. For sufficient large boson number this can be considered as a rotating condensate. In the ideal case of n non-interacting bosons one has

$$E = \Omega \left(n + \frac{5}{2} \right), \quad I = 2n, \quad (1)$$

$$B(E2, I \rightarrow I - 2) = \eta^2 \Delta \beta^2 n = \frac{1}{2} \eta^2 \Delta \beta^2 I, \quad \eta = \frac{3ZR^2}{4\pi}, \quad (2)$$

where Ω is the frequency of the d-bosons, β the Bohr deformation parameter of the Generalized Collective Model (GCM),³ and $\Delta \beta^2$ its zero point amplitude. For characterizing the energies of the tidal wave it is useful to introduce the angular frequency and the moment of inertia according to the classical relations $\omega = dE/dI$ and $J = I/\omega$, respectively,

$$\omega = \frac{\Delta E}{\Delta I} = \frac{1}{2} (E(I) - E(I - 2)), \quad J = \frac{I}{\omega}. \quad (3)$$

In the case of free bosons, $\omega = \Omega/2$ is constant. The moment of inertia J and the $B(E2)$ are proportional to I , i. e. their ratio is I -independent. This limit is indicated by the line FB (free bosons) in Fig. 3. The combination $\langle \beta^2 \rangle = \Delta \beta^2 n$ has the meaning of an average deformation. Therefore the angular momentum increases, because the moment of inertia increases $\propto \langle \beta^2 \rangle$, while the angular frequency ω is constant. In the case of a rigid rotor, J and $\langle \beta^2 \rangle$ are constant and $\omega \propto I$. Real nuclei, are between the two limits. It seems appropriate to classify the yrast states as "rotational" when the increase of I is mainly caused by an increase of ω (picket fence E_γ) and "vibrational" when it is mainly caused by an increase of J (roughly constant E_γ). The latter case is the inharmonic tidal wave mode or the rotating condensate of interacting d-bosons.

3. Phenomenology of the anharmonicity

Fig. 3 demonstrates that the yrast line of ^{102}Pd classifies as an anharmonic tidal wave. The moment of inertia is a nearly linear function of I indicated by the line IB (interacting bosons). It deviates from the harmonic limit (FB) by the small offset at $I = 0$, which is a measure of the anharmonicity. The $B(E2)$ values behave in the same way, such that the ratio $B(E2)/J$ is constant within the experimental uncertainties. The GCM suggests that both $B(E2)$ and J are $\propto \beta^2$, which implies that their ratio is I -independent.³ The available data in vibrational and transitional nuclei in the mass 100 region confirm this observation in a systematic way. Thus, one can easily

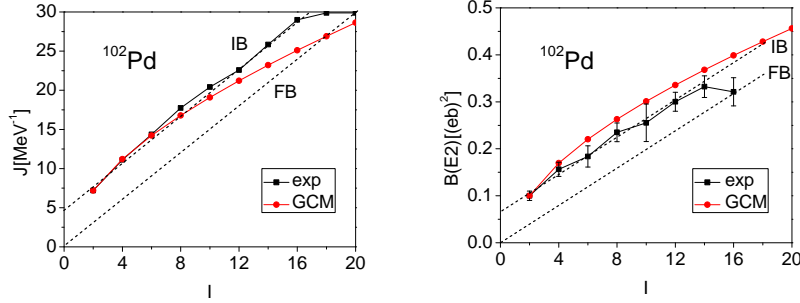


Fig. 3. The moment of inertia J (left) and the $B(E2, I \rightarrow I-2)$ transition probabilities (right) of the yrast states of ^{102}Pd . The dashed line FB (free bosons) shows the limit of harmonic bosons. The dashed line IB (interacting bosons) illustrates the near linear trend of the interacting bosons. GCM shows a calculation with the model parameters fitted to the low-lying spectrum.

predict the E2-lifetimes of the yrast levels with $I > 2$ by the relation

$$B(E2, I^+ \rightarrow (I-2)^+) = B(E2, 2^+ \rightarrow 0^+) I \frac{E_\gamma(2^+)}{E_\gamma(I^+)}. \quad (4)$$

Employing Grodzin's rule for the 2^+ states⁴

$$\frac{B(E2, 2^+ \rightarrow 0^+) [(eb)^2]}{E_\gamma [keV]} = 2.6 (eZ)^2 A^{-2/3} \quad (5)$$

one can calculate the $B(E2)$ of the yrast states from their transition energies.

The experimental $BE2, I \rightarrow I-2$ and $J(I)$ values indicate that the ground state has some deformation $\beta^2(I=0) (> \Delta\beta^2)$ which increases linearly with I . In classical terms, the tidal wave starts with a small deformation and increases its amplitude along the yrast line. In quantum language, the condensate of interacting bosons rotates like a condensate of free aligned d-bosons to which a small fraction of non-aligned d-bosons is added, which generate the I -independent part of $\beta^2(I)$. The stacking of d-bosons is seen up to $n = 7$, i.e. $I = 14$ in the left panel of Fig. 3. The $B(E2, 16_1^+ \rightarrow 14_1^+)$ belongs to the transition that connects the 16_1^+ two-quasiparticle state with the 14_1^+ seven-boson state. For $I \geq 16$ the s-configuration composed of two aligned $h_{11/2}$ quasineutrons takes over the yrast line. For $I \geq 16$, the moment of inertia $J(I)$ in the left panel is calculated from the yrast states I_2^+ . The 16_2^+ state is most likely the eight-boson state. The saturation of the curve for $I \geq 18$ indicates that the yrast states also become two-quasiparticle excitations.

4. Description by means of collective models

We investigated the anharmonicity of the tidal wave by means of the GCM version of Ref.,⁵ which involves, in addition to the quadratic, a cubic and a quartic potential. That is, the interaction between the bosons is a combination of third and fourth order terms. Ref.⁵ adjusted the potential parameters to the energy ratios between the lowest 0_2^+ , 2_1^+ , 2_2^+ , 3_1^+ , and 4_1^+ collective quadrupole excitations. A good description of the relative energies and $B(E2)$ ratios was obtained. Fig. 3 shows how the same GCM calculation describes the tidal wave, where the energies and the $B(E2)$ are scaled to the experimental values for the 2_1^+ state. The GCM reasonably well reproduces the slope and offset of the experimental curves. The ratio $B(E2, I \rightarrow I - 2)/J(I)$ is nearly I independent. However, the calculation deviates from the linear behavior of the experimental curves. This may indicate that the quartic form of the Bohr Hamiltonian is not quite appropriate.

We also attempted describing the tidal wave by means of the Interacting Boson Model (IBM 1) using parameters determined in the same way as for the GCM. IBM 1 fails to describe the multi-phonon yrast states. The function $J(I)$ is found to be decreasing, and the $B(E2)$ values decrease for $I > 6$, which is in striking contrast to experiment. The reason for the discrepancy is the cut off in boson number. According to IBM 1 counting, the maximal boson number is 5 for $Z = 46$ and $N = 56$, whereas, as discussed above, the experiment indicates the presence of the seven- and, tentatively, eight-boson states.

5. Microscopic mean field description

The tidal wave has a static deformed shape in the co-rotating frame of reference. This leads to the microscopic description suggested in Ref.,² which is based on the rotating mean field. Ref.² applied the SCTAC (shell correction tilted axis cranking) version⁶ of the Cranking Model to even-even nuclides with $44 \leq Z \leq 48$ and $56 \leq N \leq 66$. SCTAC calculates the energy for given expectation value of the angular momentum operator equal to I by means of the micro-macro method using a deformed Woods-Saxon potential. The energy is minimized with respect to the deformation parameters β and γ . Deformed solutions were found for $I \geq 2$ even when the solution was spherical for $I = 0$. These calculations describe the collective yrast states rather well. They also describe the intrusion of the aligned $h_{11/2}$ two quasi neutron states into the yrast line, which causes the back bending

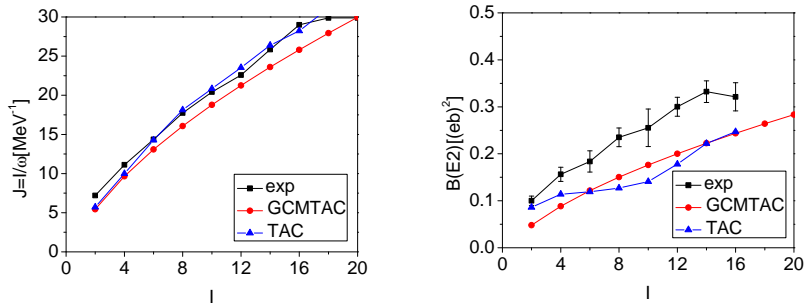


Fig. 4. The moment of inertia J (left) and the $B(E2, I \rightarrow I-2)$ transition probabilities (right) of the yrast states of ^{102}Pd . GCMTAC shows the GCM calculation with the quartic potential fitted to the microscopic TAC PES and the mass parameter adjusted to experiment. TAC is obtained by minimizing the microscopic energy with respect to the deformation parameters β and γ .

phenomenon seen in most of the studied nuclei. Figs. 4 and 5 shows two examples, which we refer to as TAC. In the case of ^{102}Pd , the function $J(I)$ is very well reproduced. The $B(E2)$ values show the characteristic increase with I . However, their absolute values is too small. Note, there are no adjustable parameters in the calculation. Of course, one could achieve good agreement with experiment by introducing an effective charge. In the case of ^{110}Cd , the TAC function $J(I)$ (not shown) agrees very well with experiment. At $I = 12$, the aligned $h_{11/2}$ two-quasi neutron configuration becomes yrast, which is very accurately reproduced by the TAC calculation. As seen in Fig. 5, the TAC calculation underestimates the $(BE2)$ values of the tidal wave branch $I \leq 10$. The drop at $I = 12$ indicates the change to the $h_{11/2}$ two-quasineutron configuration, the $B(E2)$ values of which are well reproduced. The TAC calculations of Ref.² give also too small $B(E2)$ values in the tidal branches of ^{104}Ru and $^{106-110}\text{Pd}$, for which lifetimes have been measured up to $I = 8$.

6. Mixed description

The TAC calculations treat the quadrupole degree of freedom in a classical way, which disregards zero point fluctuations. In order to take them into account, we fitted the quartic potential of GCM Hamiltonian to the $I = 0$ potential energy surface (PES) calculated by means of TAC. Fig. 6 shows the fit for axial shapes. The mass parameter $B = 90\hbar^2 \text{ MeV}^{-1}$ of the GCM was adjusted to the experimental energy scale. The factor η in Eq. (2) was used to connect the deformation parameter β with the $B(E2)$. This relation

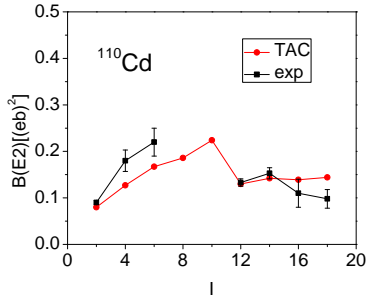


Fig. 5. The $B(E2, I \rightarrow I - 2)$ transition probabilities of the yrast states of ^{110}Cd . TAC is obtained by minimizing the microscopic energy with respect to the deformation parameters β and γ .

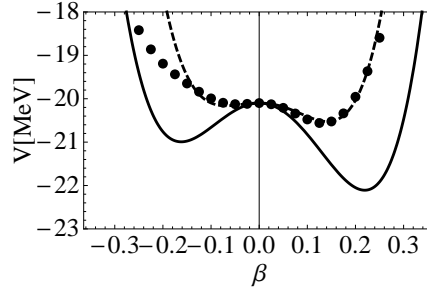


Fig. 6. Ground state potentials of ^{102}Pd . Dots: microscopic TAC potential, dashed curve: quartic GCM potential fitted to the dots, full curve: phenomenological GCM potential.

is very close to the microscopic relation in the TAC calculations. The results obtained with this GCM Hamiltonian are denoted by GCMTAC in Fig. 4. The function $J(I)$ is well reproduced. The $B(E2)$ values are too small. It is surprising that results of the TAC and the GCMTAC calculations are very similar, that is, that the inclusion of the zero point fluctuations seems not to lead to dramatic changes.

The small $B(E2)$ values of the TAC and GCMTAC calculations can be traced to the micro-macro TAC PES. As seen in Fig. 6, the potential of the phenomenological GCM Hamiltonian, which reproduces the $B(E2)$ well, is much wider. We investigated a number of parameter sets from the literature for the Woods-Saxon potential used in the SCTAC calculations. The resulting PES were similar to the one in Fig. 6 and the $B(E2)$ values too small. Adopting the Nilsson potential did not resolve the problem. On the other hand, the agreement of the calculated $B(E2)$ values with experiment in ^{110}Cd for $I \geq 12$ gives credibility to the TAC PES. The CNS model⁷ and the TRS calculations⁸ reproduce energies and $B(E2)$ values of high spin states of many nuclei, including the discussed ones. CNS and TRS apply the micro-macro method based on the Nilsson and Woods-Saxon potentials, which gives additional strong credibility to the TAC PES. At this point, it remains unclear why the microscopic approach underestimates the $B(E2)$ values of the tidal wave.

7. Summary

The states of highest d-boson number will be found along the yrast line. The seven-phonon yrast state has been identified in ^{102}Pd . The semi-classical concept of a tidal wave running over the nuclear surface characterizes the nature of the d-bosonic yrast states. The boson interaction generates anharmonicity, which shows up as a constant shift of the $B(E2, I \rightarrow I - 2)$ value and the moment of inertia $J(I)$ as functions of the spin. The ratio $B(E2, I \rightarrow I - 2)/J(I)$ is found to be approximately I -independent, which allows one to predict the $B(E2)$ values from the yrast energies. A collective Hamiltonian with a quartic potential, the parameters of which were adjusted to low-lying collective states, accounts well for the experimental energies and $B(E2)$ values in ^{102}Pd . Microscopic calculations without adjustable parameters, based on the Cranking Model, reproduce the energies, but underestimate the $B(E2)$ values by a factor of about $2/3$.

Acknowledgments

Supported by the DoE Grant DE-FG02-95ER4093. We thank A. D. Ayangeakaa and U. Garg for making the lifetime data available to us.

References

1. D. Ayangeakaa, U. Garg *et al.* private communication, to be published
2. S. Frauendorf, Y. Gu, and J. Sun, *Int. J. Mod. Phys. E* **20**, 425 (2010), online arXiv:1109.1842.
3. J. M. Eisenberg and W. Greiner, in *Nuclear Theory, Vol. I* (North Holland, Amsterdam, 1987).
4. S. Raman *et al.*, *Atomic Data and Nuclear Data Tab.* **78**, 1 (2001).
5. M. A. Caprio, *Phys. Rev. C* **68**, 054303 (2003).
6. S. Frauendorf, *Nucl. Phys. A* **677**, 115 (2000).
7. A. Afanasjev *et al.* *Phys. Rep.* 322, 1 (1999).
8. R. Wyss in *Nuclear Structure Models* (World Scientific, Singapore, 1992).